J. Fluid Mech. (2006), *vol.* 554, *pp.* 67–83.
doi:10.1017/S0022112006009074 Printed in the United Kingdom

Multiscale modelling in the numerical computation of isothermal non-wetting

By MARC K. SMITH AND G. PAUL NEITZEL

The George W. Woodruff School of Mechanical Engineering,
Georgia Institute of Technology, Atlanta, GA 30332-0405, USA

(Received 17 August 2005 and in revised form 16 January 2006)

A state of permanent, isothermal non-wetting of a solid surface by a normally wetting liquid may be achieved if the surface moves tangentially to a liquid drop that is pressed against it. Surrounding gas is swept into the space between the liquid and solid creating a lubricating film that prevents wetting. The length scales of the drop and the film are typically three or more orders of magnitude different, making numerical simulation difficult from a resolution standpoint. The present paper focuses on a hybrid approach employing lubrication theory for the thinnest portions of the gas film and numerical simulation for the liquid and outer gas phases.

1. Introduction

Reported observations of drops of a single liquid that bounce off one another without coalescing or off solid surfaces without wetting date back at least as far as those of Lord Rayleigh (1879), who discussed the "rebound of drops when they come into collision with one another". Temporary non-coalescence, such as observed by Rayleigh with his colliding water jets, is important in phenomena such as raindrop coalescence and droplet combustion.

Recently, the subject of permanent non-coalescence and non-wetting has become of interest. In these cases, a lubricating film of gas is driven between the liquid–liquid or liquid–solid surfaces, keeping them sufficiently far apart that attractive van der Waals forces remain weak. So long as the lubricating gas film is supplied, the surfaces remain separated, leading to the permanence of the event. A recent review by Neitzel & Dell'Aversana (2002) discusses work done on both temporary and permanent non-coalescence and non-wetting.

Two mechanisms have been identified thus far for providing the lubricating film for the permanent cases. Thermocapillarity, coupled with a temperature difference between the two surfaces in question, may be used to supply the lubricating gas. The second mechanism, termed isothermal non-coalescence/non-wetting, drives the gas film by one surface being in a state of motion tangential to the other, such as through pressing a liquid drop against a rotating liquid bath or solid disk.

Apart from their intrinsic characteristics, interest in permanent non-coalescence and non-wetting stems from the potential utility of such systems in practical applications ranging from micro-electro-mechanical systems (MEMS) and lab-on-a-chip (LOC) to microgravity systems for Space uses. This utility is realized, in part, by the fact that these systems are able to carry loads in excess of drop weights and by the existence of low friction between a non-wetting drop and surface, enabling enhanced liquid transport from point to point on a surface. Dell'Aversana & Neitzel (2004) have measured

loads for thermocapillary non-wetting drops pressed against cooled surfaces and have shown that the load-carrying ability is due to the increase in capillary pressure within the drop as it is squeezed against the unwetted surface. The successful application of robust versions of such systems requires a detailed understanding not only of their load-carrying capacities, but also of the conditions under which such systems are likely to fail. Such knowledge can be gained by experiment, and by careful numerical simulations of the flow fields within both the liquid drop and the lubricating gas film.

One difficulty in simulating the flow fields associated with non-coalescing and non-wetting systems concerns the disparate length scales associated with flows within the liquid and gas phases. Drops employed in experiments are typically of millimetre size while the gas films, which may be measured with interferometry (Dell'Aversana, Tontodonato & Carotenuto 1997), are three orders of magnitude smaller. If the discretization level in a numerical model is maintained over these two regions, the disparate length scales inflate the problem size in the thin region by a factor of one thousand in a two-dimensional simulation and a factor of one million in a three-dimensional simulation. Such large problems are very difficult to solve with current computing hardware.

Previous simulations of the thermocapillary non-wetting problem employ simplistic models of the film region, use assumptions regarding the drop that are not relevant to proposed applications, or are unable to obtain solutions for realistic configurations. For example, the numerical simulations of Monti & Savino (1997) and Savino & Monti (1997) assumed a liquid free-surface shape determined by the static Young–Laplace relation to compute thermocapillary flow within the drop; the surface speed thusly obtained was used to compute the gas flow in an axisymmetric channel of constant height, as opposed to the dimpled surface measured by Dell'Aversana *et al.* Sumner, Wood & Neitzel (2003) performed a lubrication analysis of the flows in both the liquid and gas phases, necessarily assuming a 'flat' drop instead of using a shape more relevant to the experimental work, in which the initial shape is closer to hemispherical. Chen, Kuo & Neitzel (2006) used the commercial code FIDAP to compute liquid and gas flows associated with thermocapillary non-wetting of a two-dimensional drop. They meshed the entire flow field, including the lubricating gas film under the drop, but were unable to obtain solutions when the gas film was extremely thin.

The present work addresses the isothermal non-wetting problem. If the drop holder and the moving plate are held at the same temperature, the isothermal assumption is valid provided that viscous heating in the gas film is small. A balance of heat diffusion in the film to viscous heating produces the relation $\Delta T = \mu U^2/k$, where ΔT is the temperature difference across the film, μ and k are the dynamic viscosity and thermal conductivity of the gas, and U is the speed of the plate. An experimental velocity of $46\,\mathrm{cm\,s^{-1}}$ (see figure 1) and standard properties for air yields $\Delta T = 0.15\,\mathrm{mK}$. Thus, the isothermal assumption is reasonable.

Neitzel & Dell'Aversana (2002) have shown that isothermal non-wetting is possible for silicone-oil drops pressed against disks rotating with a local tangential speed sufficient to supply the lubricating film. Because of the existence of a preferred flow direction within the film, the axisymmetry observed in thermocapillary non-wetting is not preserved. Rather, the flow within both the drop and film exhibit mid-plane symmetry, as seen in the interferogram and reconstructed interface shape presented in figure 1.

Although a two-phase lubrication analysis of the type performed by Sumner *et al.* (2003) is also possible for this system, the present work will seek a solution that does

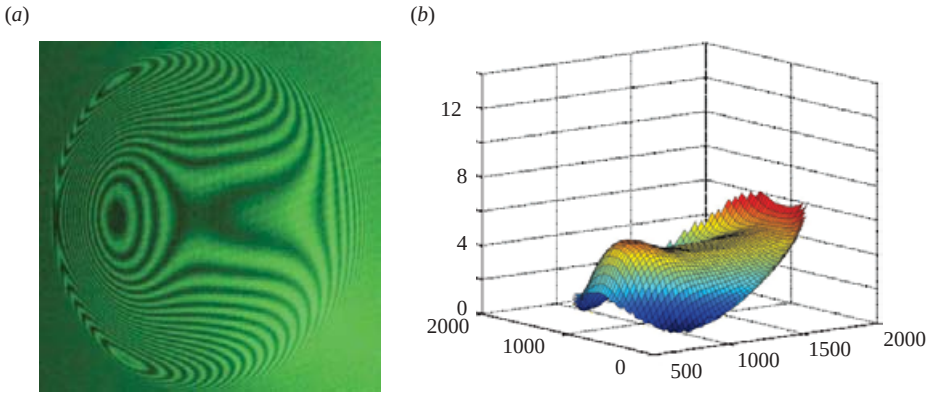

FIGURE 1. (*a*) Interferogram and (*b*) reconstructed liquid-surface shape (dimensions in μm) for an isothermal, non-wetting silicone-oil drop pressed against a rotating disk. Tangential speed (right-to-left) of the disk is $46\,\mathrm{cm\,s^{-1}}$ Neitzel & Dell'Aversana (2002).

not require a flat drop through the use of a hybrid lubrication-theory/computational-fluid-dynamics (CFD) approach. Kuo, Chen & Neitzel (2005) used their FIDAP model to compute full CFD solutions for this case, but could not obtain solutions for extremely thin lubricating films, just as in the thermocapillary non-wetting problem discussed above.

There have been previous hybrid approaches to solving fluid-flow problems that focused on the use of different techniques in different regions of the flow where length scales change greatly. One such problem occurs during the process of forward roll coating. Ruschak (1982) used lubrication theory for the one-dimensional flow in the gap, matched to finite-element solutions of the two-dimensional Navier–Stokes equations in the downstream region where the film splits, enabling the correct computation of the film-splitting point. Hadjiconstantinou (1999) treated the moving contact line by applying a molecular-hydrodynamics solution in a neighbourhood of the line coupled with a continuum hydrodynamics approach away from this location. The use of overlapping domains and the implementation of boundary conditions through a variation of the domain-decomposition Schwarz alternating method enabled hybrid solutions to be obtained. Stay & Barocas (2003) applied a Galerkin finite-element technique to compute Stokes flow in the vicinity of a thin region and coupled the results to a lubrication solution in the thin region. The technique was illustrated with a deformable roll-coating geometry.

The hybrid method formulated in the present work uses a finite-element-based CFD approach in regions of macroscopic length scale coupled to an asymptotic lubrication analysis in the microscale region. A departure from earlier approaches relates to the fact that the microscale region is bounded by two fluid phases in need of a solution, namely the macroscopic-scale gas flow at the inlet and exit to the lubrication film and the macroscopic liquid flow that is driven through the interfacial stress due to both the moving gas in the film as well as that in the bulk regions.

The model problem considered is this work is an isothermal, two-dimensional liquid drop attached to a solid planar surface and pressed against a lower moving solid surface so that non-wetting is observed. For the three-dimensional case shown in figure 1, the approaching gas is able to pass laterally around the drop as well as beneath it within the lubrication region. For the two-dimensional case considered here, lateral motion is impossible. Furthermore, one would expect that not all of the

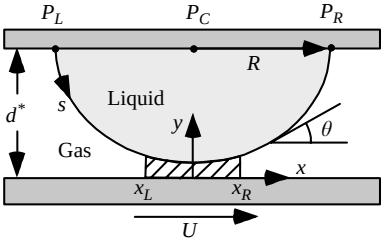

FIGURE 2. Schematic of the problem geometry.

approaching gas would be able to pass through the lubrication region, leading to a blockage and a resulting flow ahead of the drop in a direction opposite to that of the plate motion. Such two-dimensional isothermal non-wetting would be observed, for example, in the interior region (i.e. away from the ends) of a 'thread' of fluid sliding perpendicular to its long axis along a solid surface. Two-dimensional isothermal non-wetting has not been demonstrated experimentally, but its thermocapillary counterpart has (Nalevanko 1997).

The problem formulation and an outline of the solution procedure are given next in § 2. Results are found in § 3 and the paper concludes with a discussion in § 4.

2. Problem formulation and solution procedure

2.1. *Geometry and dimensionless parameters*

Consider two parallel, solid, planar surfaces of infinite horizontal extent spaced a distance d^* apart, as sketched in figure 2. The upper surface is fixed and the lower surface moves to the right at a speed U in its own plane. A two-dimensional liquid drop is attached to the underside of the upper surface, pinned at points P_L and P_R spaced a distance $2R$ apart. The drop is composed of an incompressible viscous liquid with a volume per unit length (or area) A^*. An incompressible viscous gas bounds the exposed portion of the drop and fills the rest of the space between the two solid surfaces. In the present model, the two fluids are assumed to be isothermal. A Cartesian coordinate system is used with the x-axis lying in the lower surface and the y-axis passing through point P_C, the mid-point of the line segment $\overline{P_L P_R}$.

The motion of each fluid is governed by the Navier–Stokes and continuity equations, in which gravity is ignored. The liquid–gas interface is a simple, deformable interface with surface tension σ. Standard interfacial boundary conditions are used, i.e. continuity of velocity and tangential stress, the kinematic constraint that the normal interfacial velocity equals the normal fluid velocity, and a normal-stress difference equal to the surface tension times interfacial curvature. For brevity, these equations are not reproduced here.

The governing equations are scaled using length, velocity, pressure, and time scales of R, U, ρU^2, and R/U, respectively. The primary dimensionless parameters that result are the solid-surface separation distance $d = d^*/R$, drop area $A = A^*/(\pi R^2/2)$, density ratio $r = \rho_l/\rho_g$, viscosity ratio $m = \mu_l/\mu_g$, Reynolds number $Re = \rho_g U R/\mu_g$, and Weber number $We = \rho_g U^2 R/\sigma$, where g and l subscripts refer to gas and liquid, respectively.

In the present work, the only drop area considered is $A = 1$. Thus, if the two fluids are motionless (with $U = 0$) and the solid-surface separation distance $d > 1$, the drop does not touch the lower surface, it has a semicircular shape, and both contact angles are 90°.

	ρ (g cm^{-3})	μ (g cm^{-1} s^{-1})	σ (g s^{-2})
Silicone oil	0.91	0.0455	19.2
Air	0.00121	0.1528×10^{-3}	—

TABLE 1. Material properties for silicone oil and air.

The fluid motion in this system is driven by the translation of the lower surface and a pressure gradient applied in the x-direction. Far away from the drop in both the positive and negative x-directions the flow is assumed to be a simple Couette–Poiseuille parallel flow given in dimensionless form as

$$\left.\begin{aligned} u &= \frac{K}{2}(y^2 - yd) + 1 - \frac{y}{d}, \\ K &= 6\,(d - 2q)/d^3. \end{aligned}\right\} \tag{2.1}$$

Here, K is the dimensionless pressure gradient in the flow scaled using the viscous stress in the gas. The parameter $q = q^*/(RU)$ is the dimensionless volume flow rate of the gas between the two solid surfaces. The two parameters q and K are not independent. In this work, the flow rate q is chosen as the primary parameter characterizing the flow far from the drop.

As now posed, this problem is characterized by seven independent parameters: r, m, Re, We, A, d, and q. For a given liquid–gas combination r, m, and We/Re^2 are determined. Setting the speed U of the lower surface then determines Re and We. Thus, the goal of the present work is to find steady solutions for the flow in the gas and the liquid and the shape of the drop as functions of the solid-surface separation distance d, the flow rate of the gas q, and the Reynolds number Re. The default parameter set used for all results reported in this work are for 4.55 cSt silicone oil and air and a lower-surface translation speed of 30 cm s^{-1}, corresponding to the simulations of Kuo *et al.* (2005). The material properties are listed in table 1. The dimensionless parameters are $r = 752.07$, $m = 297.77$, $We/Re^2 = 0.10050 \times 10^{-4}$, $Re = 23.756$, and $We = 0.56719 \times 10^{-2}$.

The lubrication domain beneath the drop is indicated by the small hatched region in figure 2. This is where the drop is closest to the lower surface and the lubricating gas film flow is important. The hybrid numerical scheme developed to solve this problem is composed of three separate parts: (i) a finite-element model used to solve for the flow away from the lubrication domain, (ii) an asymptotic solution for the gas flow in the lubrication domain; and (iii) a drop-shape computation based on the normal-stress balance on the drop interface. The following subsections describe each of these parts and their integration into the final hybrid model.

2.2. *The finite-element model*

The flow problem away from the lubrication domain is easily modelled using the finite-element method, implemented with the software FEMLAB 3.1. One limitation of FEMLAB 3.1 is that it does not handle deformable-interface problems. This was overcome by writing a MATLAB function to iteratively compute the drop shape based on the normal-stress jump on the liquid–gas interface obtained from a flow computation for a given drop shape, as described later in § 2.4.

The flow domains for the FEMLAB model are shown in figure 2. A finite channel of height d and width w is defined for the gas flow. The drop interface is defined by a curve obtained from a cubic-spline interpolation of a set of uniformly spaced points

along the drop circumference, including the contact lines at points P_L and P_R. The flow domain does not include the hatched lubrication domain.

FEMLAB's Incompressible Navier–Stokes, steady-state-analysis, application mode is used to define separate sets of governing equations for each fluid phase, which are coupled through the interfacial boundary conditions. Continuity of velocity is satisfied by setting the velocity of the gas equal to the velocity of the liquid at the drop interface. Continuity of tangential stress is enforced by using FEMLAB's slip boundary condition on the drop surface for the liquid. Thus, all of the appropriate boundary conditions on the drop interface are satisfied, except for the normal-stress balance; this condition is implicitly satisfied when the correct drop shape is found.

The remaining boundary conditions in the FEMLAB model are set as follows. Kinematic and no-slip conditions are applied at the upper and lower solid surfaces. On the left and right ends of the channel, a parallel flow is specified using equation (2.1) for the horizontal velocity and setting the vertical velocity to zero. The pressure levels in the gas domains on the left and right sides of the channel are specified by setting the pressure on the drop interface at the left and right sides of the lubrication domain to values obtained from the lubrication flow. Finally, the pressure level in the drop is specified by setting the pressure at point P_C on the upper surface to p_{drop}. In the full deformable-interface problem, p_{drop} is an unknown and is determined as part of the solution. However, the value of this unknown pressure does not affect the finite-element model at this level because the normal-stress boundary condition is not imposed at this time.

The fluid domains are meshed using triangular Lagrange quadratic elements with a maximum element size limited to 0.1. On the drop boundary, the maximum element size is limited to 0.02, while at the contact lines the element size is limited to 0.01. Along the drop boundary, the element growth rate moving away from the boundary is set to 1.03. For $d > 1.02$, a lubrication domain is not required and a typical simulation (with $d = 1.02$) has approximately 12 000 elements and 56 000 degrees of freedom. An average computation of this size with an error tolerance of 10^{-6} takes approximately 38 s to complete on a 3 GHz Windows computer with 1 GB of memory.

Mesh convergence was checked for $d = 1.02$ and no lubrication domain by halving the element size limit on all domains, boundaries, and points. The change in quantities such as the x- and y-forces on the drop, the maximum velocity on the drop interface, and the maximum and minimum pressures under the drop was less than 0.55%. This was considered an acceptable accuracy and so the original mesh parameters given above are used for the remainder of the results reported in this work.

The solid surfaces in the model problem are of infinite horizontal extent. In the numerical model, these surfaces were necessarily limited to a finite channel of width w. Simulations were done with channel widths of 6, 8, and 16 using the same mesh parameters. The differences in the quantities mentioned above between channels with widths of 8 and 16 were less than 0.02%, with only the maximum pressure under the drop in error by 0.26%. For channel widths of 6 and 16, errors were less than 0.15%, with only the maximum pressure off by 0.55%. A channel width of $w = 8$ was conservatively chosen so that end effects on the flow around the drop are negligible.

2.3. *The lubrication model*

The velocity field in the lubricating gas film is described using lubrication theory. The lubrication domain is given by $\{(x, y)|x_L \leqslant x \leqslant x_R, 0 \leqslant y \leqslant h(x)\}$, where x_L and x_R are the locations of the left and right boundaries respectively, and $h(x)$ is the location

of the drop interface. The interface is a non-deformable surface on which the gas velocity is equal to the liquid velocity, just as in the FEMLAB model discussed above.

The leading-order lubrication equations for two-dimensional steady flow in the lubrication domain are written in primitive dimensional variables with standard notation as

$$-p_x + \mu_g u_{yy} = 0, \tag{2.2a}$$

$$-p_y = 0, \tag{2.2b}$$

$$u_x + v_y = 0, \tag{2.2c}$$

where x and y subscripts denote partial differentiation. The corresponding boundary conditions are

$$u(y=0) = U, \quad u(y=h) = U_d, \tag{2.3a,b}$$

$$p(x=0) = 0, \tag{2.3c}$$

$$v(y=0) = 0, \tag{2.3d}$$

$$v = V_d, \quad v = uh_x, \quad \text{on } y = h. \tag{2.3e,f}$$

Here, U_d and V_d in boundary conditions (2.3b, e) are the velocity components of the liquid at the drop interface. These two conditions make the gas and liquid velocity fields at the drop interface continuous. Note that the liquid velocity from the FEMLAB model is tangential to the drop interface and so it satisfies the kinematic condition. Thus, conditions (2.3b, e, f) form a dependent set. Since only one boundary condition is needed to find the vertical velocity, condition (2.3e) can be safely dropped. The pressure level in the gas is defined by setting the pressure at the origin to zero in condition (2.3c).

Equation (2.2b) shows that $p = p(x)$. This result allows the integration of the momentum equation (2.2a), which after applying boundary conditions (2.3a, b), yields the horizontal velocity

$$u = \frac{Kh^2}{2}\left(\frac{y^2}{h^2} - \frac{y}{h}\right) + (U_d - U)\frac{y}{h} + U, \tag{2.4}$$

where $K(x) \equiv p_x/\mu_g$.

From the continuity equation (2.2c) and the horizontal velocity (2.4), the vertical velocity is determined to be

$$v = -\frac{K_x h^3}{2}\left(\frac{y^3}{3h^3} - \frac{y^2}{2h^2}\right) + \frac{Kh_x y^2}{4} - \frac{(U_d)_x\, y^2}{2h} + \frac{(U_d - U)\, h_x y^2}{2h^2}. \tag{2.5}$$

The pressure in the lubrication domain is obtained by integrating the continuity equation (2.2c) with respect to y over the thickness of the gas film. Defining the volume flow rate in the gas as $q = \int_0^{h(x)} u\,\mathrm{d}y$ and using the kinematic condition (2.3f) yields the condition $q_x = 0$, which leads to the fact that q is constant. Integrating the horizontal velocity over the film thickness gives an equation for the flow rate. Solving this for K and using the definition $K(x) \equiv p_x/\mu_g$ produces the pressure gradient

$$p_x = \mu_g \left\{\frac{6\,(U_d + U)}{h^2} - \frac{12q}{h^3}\right\}. \tag{2.6}$$

The pressure gradient is integrated numerically for a given shape of the drop interface $h(x)$ as described below.

The final quantity needed from the lubrication model is the shear stress of the gas at the drop interface, defined to leading order as $\tau = \mu_g u_y(h)$. Using the horizontal

velocity (2.4) produces the result

$$\tau = \mu_g \left\{ \frac{Kh}{2} + \frac{(U_d - U)}{h} \right\}. \tag{2.7}$$

The analytical expressions for the velocity components and the shear stress on the drop interface in the lubrication domain are combined with the FEMLAB model as follows. In the FEMLAB geometry, the hatched lubrication domain shown in figure 2 is not meshed. In its place, the velocity components in the lubrication domain given by equations (2.4) and (2.5) are used as velocity boundary conditions at $x = x_L$ and $x = x_R$. The shear stress from equation (2.7) is applied to all liquid elements that border the lubrication domain using a weak formulation.

The lubrication pressure is coupled to the FEMLAB model by creating a one-dimensional FEMLAB geometry equivalent to the line segment (x_L, x_R), which is the lower boundary of the lubrication domain. FEMLAB's PDE, Coefficient Form, application mode is used in this geometry. The coefficients and boundary conditions of the PDE are chosen to produce the following first-order ODE and boundary condition:

$$\frac{\mathrm{d}p}{\mathrm{d}x} = p_x, \quad p(0) = 0. \tag{2.8a, b}$$

Integration of system (2.8) yields the lubrication pressure. The pressure gradient (2.6) defined in the first geometry is coupled to the second geometry and the pressure from the second geometry is coupled to the first geometry on both the upper and lower boundaries of the lubrication domain by defining FEMLAB extrusion coupling variables. Lastly, the pressure in the gas on the drop interface at the left and right boundaries of the lubrication domain is set equal to the lubrication pressure at these same points.

The FEMLAB model of the flow outside the lubrication domain produces a small variation in the gas pressure between the drop interface and the lower solid surface at both ends of the lubrication domain. This difference is not resolved in a leading-order lubrication theory since from equation (2.2*b*) the lubrication pressure is constant across the thickness of the lubrication domain. Since the pressure coupling process makes the pressure continuous along the drop interface, there are small pressure discontinuities on the lower surface at both ends of the lubrication domain. These discontinuities were removed by adding a small linear correction to the lubrication pressure on the lower surface in the lubrication domain. As a result, the zero-pressure reference point on the lower surface is slightly displaced from the origin. The true zero-pressure reference point in the gas lies at the intersection of the drop interface and the y-axis.

The coupling of the lubrication model and the finite-element model is completed by locating the ends of the lubrication domain x_L and x_R at the points where the drop interface slope is $\mp 15^\circ$ from the horizontal, respectively. This slope value was chosen by comparing the results from a FEMLAB computation without a lubrication model to those with one and varying the location of the ends of the lubrication domain over drop interface slopes from 2° to 30°. The comparison uses parameters for silicone oil and air from table 1, $d = 1.02$, $q = 0.014$, and $Re = 23.756$. The differences in the results for the horizontal force on the drop and the effective pressure drop across the drop are minimized at a slope angle of 15°, being 2.4% and -0.8% respectively. Unfortunately, the difference in the vertical force on the drop is maximized at this slope angle at a

value of −13.3%. Despite this, these differences were deemed acceptable and a slope angle of 15° was used in all subsequent computations reported in this work.

2.4. *The drop-shape computation*

The properties of the two-dimensional curve describing the drop interface are easily characterized using an arc-length coordinate system as shown in figure 2. The arc-length s along the curve is measured from the left-hand contact line at point P_L. Each point on the curve is given by a position vector $\boldsymbol{R}$ with respect to point P_C. Corresponding to each interfacial point is a Cartesian position (x, y), a slope θ measured counterclockwise from the x-axis, and a curvature κ, defined as positive when the slope increases with arc-length. As the position vector moves along the interface, it sweeps out an area a. The position, slope, and curvature of the interface and the swept area are functions of the arc-length only, determined by the following system of four first-order ODEs:

$$\left.\begin{aligned} &\frac{\mathrm{d}x}{\mathrm{d}s} = \cos\theta, \quad \frac{\mathrm{d}y}{\mathrm{d}s} = \sin\theta, \quad \frac{\mathrm{d}\theta}{\mathrm{d}s} = \kappa, \\ &\frac{\mathrm{d}a}{\mathrm{d}s} = \frac{1}{2}\left(x\sin\theta - (y-d)\cos\theta\right). \end{aligned}\right\} \tag{2.9}$$

The six boundary conditions for the drop-shape equations are

$$\left.\begin{aligned} &x(0) = -1, \quad x(s_0) = 1, \\ &y(0) = d, \quad y(s_0) = d, \\ &a(0) = 0, \quad a(s_0) = \pi A/2, \end{aligned}\right\} \tag{2.10}$$

where s_0 is the unknown arc-length at the right-hand contact line and A is the dimensionless area of the drop defined in § 2.1. The remaining unknown in this set of equations is the drop pressure p_{drop}, which appears in the dependence of the curvature κ on the pressure and flow fields in the system, as described next.

The local curvature (and thus the drop shape) is determined from the normal-stress balance on the liquid–gas interface. The dimensionless form of this equation is

$$\kappa = We\,(ns_g - ns_l + p_{drop}), \tag{2.11}$$

where *ns* refers to normal stress, g and l subscripts refer to gas and liquid respectively, and the drop pressure level p_{drop} has been explicitly separated from the remainder of the normal stress in the liquid ns_l. For $d > 1$, $A = 1$, and a motionless lower surface, the static drop shape is a semicircle with a radius of one. From equation (2.11), the constant curvature of the drop $\kappa = 1$, leads to $p_{drop} = 1/We$, which in dimensional form is σ/R, the capillary pressure.

When the speed of the lower surface is non-zero, the drop-shape computation is done numerically. First, the flow field in the system is determined by solving the finite-element/lubrication-theory model for a given drop shape. The normal stresses on the drop interface in the gas and the liquid are extracted from these results to form the right-hand side of equation (2.11). System (2.9), with forcing provided by equation (2.11), is then solved as an initial-value problem with the MATLAB function *ode45* using the three initial conditions of (2.10), an initial guess for the slope,

$$\theta(0) = \theta_0, \tag{2.12}$$

and an error tolerance of 10^{-6}. The equations are integrated to $y = d$. Two nested iteration loops are used to determine the values of θ_0 (outer iteration) and p_{drop}

(inner iteration) necessary to obtain the correct right-hand contact-line position and drop area, respectively, to an error tolerance of 10^{-5}. At the end of this process, a new drop shape satisfying all six boundary conditions (2.10) is known along with a corresponding new value for the drop pressure level.

2.5. *FEMLUB*

The numerical solution of the full deformable interface problem sketched in figure 2 is performed using a MATLAB program called FEMLUB in which the finite-element/lubrication-theory flow model and the drop-shape computation are executed in a simple iteration loop. The loop calls two interior MATLAB functions. The inputs to the first function are the problem parameters, the (x, y)-coordinates of a guess for the drop shape, and a guess for the drop pressure level. This function sets up the geometry of the system for the given drop shape, formulates the coupled flow models described in § 2.2 and § 2.3, and solves for the entire flow field using FEMLAB. It returns the normal-stress jump at the drop interface given by equation (2.11). The second function uses the normal-stress jump as an input and returns the new drop shape and drop pressure level as described in § 2.4. The iteration loop is terminated when the maximum displacement over all points describing the drop shape and the relative change in the drop pressure level are less than 2×10^{-4}.

When the surface separation distance d is too close to one, convergence problems appear in the FEMLUB iteration loop as a result of the drop-shape computation. Given a reasonable drop shape, FEMLAB easily computes the flow field from the finite-element/lubrication-theory model for any surface separation distance. However, in some parameter ranges and when $d < 1.02$, the new drop shape computed from the normal-stress jump would either intersect the lower surface or fail to intersect the upper surface. In other parameter ranges, the drop-shape computation was successful but as the iteration proceeded the drop interface would oscillate between two different shapes. These difficulties occur when the drop is very close to the lower surface because both the global flow field and the drop shape become very sensitive to the gas flow in the lubrication domain beneath the drop. The lubrication pressure becomes so large that a small change in the film thickness for a fixed flow rate causes a large change in the lubrication pressure. It is these large pressure changes that cause the failure of the normal-stress integration for the drop shape and/or drop-shape oscillations during the iteration process.

Two modifications to the iteration procedure are used to address these problems. The first is to change the flow rate in the channel from a constant value to one linearly dependent on the minimum thickness in the lubrication domain h_{min}, i.e. $q = kh_{min}$; this corrects most of the oscillation problems. The second modification is to add two layers of relaxation to the iteration loop. First, the absolute and relative changes in the normal-stress jump anywhere on the drop interface are not allowed to exceed 0.05 or 5%, respectively. Second, changes in the positions of the points defining the drop interface geometry and the pressure p_{drop} in the drop are relaxed in the normal fashion, i.e. $x_{i+1} = x_i + \beta(x_{i+1} - x_i)$ for some variable x. The relaxation parameter β is set to a value of 0.25 when the normal-stress jump is relaxed and to a value of 0.5 when the changes in the normal stress are so small that relaxation of the jump is not needed. For separation distances $d < 1$, the relaxation parameters are 0.01 for the normal-stress change and 0.05 for the shape change. Note that these values for the relaxation parameters may not be optimal and that both forms of relaxation are needed to ensure successful iterations when the separation distance is less than one.

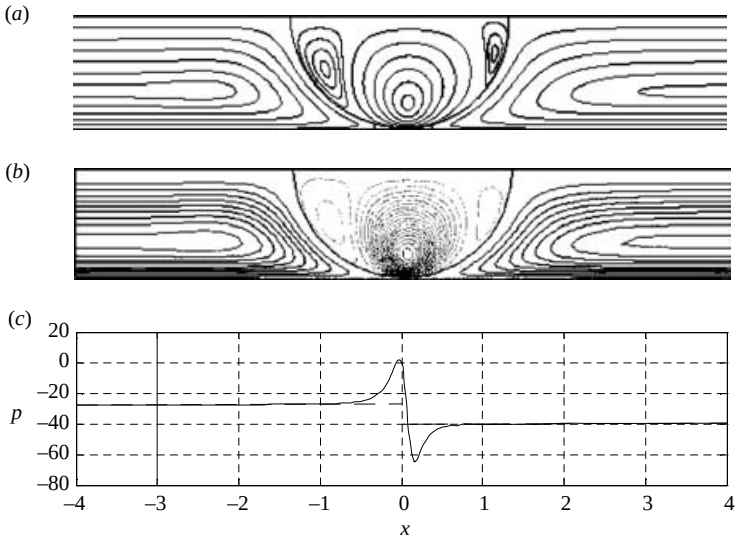

FIGURE 3. The flow field for a silicone-oil drop and air with $d = 1.01$, $Re = 23.756$, and $q = 0.00860$. (*a*) Streamlines from the FEMLUB model, (*b*) streamlines with an estimated flow rate $q = 0.0085 \pm 0.0003$ from the FIDAP model by Kuo *et al.* (2005), and (*c*) pressure along the lower surface from the FEMLUB model.

3. Results

In the following results, the drop is silicone oil with a dimensionless area $A = 1$ and the gas flowing past the drop is air. The primary parameters for investigation are the separation distance d, the Reynolds number Re, and the flow rate q. Figure 3(*a*) shows the streamlines for the flow when $d = 1.01$, $Re = 23.756$, and $q = 0.00860$. Away from the drop at each end of the channel the flow is parallel with a Couette–Poiseuille velocity profile and a constant pressure gradient. Most of the gas entering the channel on the left side moves along the bottom surface, turns around near the drop, and exits the channel on the left side along the top surface. On the right side of the channel, gas enters along the top surface, turns around near the drop, and exits along the bottom surface. The maximum velocity in the gas for this flow rate is always at the lower moving surface, a dimensionless value of $u = 1$. The flow in the liquid has a very small magnitude because of the large liquid/gas viscosity ratio. A strong primary counter-clockwise vortex occurs near the centreline of the drop, driven by the shear stress from the gas in the lubrication domain beneath the drop. Two weaker clockwise vortices exist on either side of the primary vortex and are driven partly by the shear stress of the gas as it flows alongside the drop. The left vortex is larger and stronger than the right one because the gas is being forced under the drop by the moving plate on the left side. The maximum velocity in the liquid occurs at the drop interface in the primary vortex. For comparison, the local extrema of the tangential velocity V_s on the drop interface are $V_s = 0.0419$ for the primary vortex, $V_s = -0.26 \times 10^{-2}$ for the left vortex, and $V_s = -0.60 \times 10^{-3}$ for the right vortex. Note that the drop is pushed slightly to the right so that the left contact angle is $\theta_L = 87.7^\circ$.

Streamlines for the flow field from the FIDAP model by Kuo *et al.* (2005) are shown in figure 3(*b*). Their computation had the same spacing $d = 1.01$ and $Re = 23.756$ (a lower surface speed of $U = 300\,\mathrm{mm\,s^{-1}}$). A flow rate estimate from Kuo *et al.*'s results is $q = 0.0085 \pm 0.0003$, while the FEMLUB model has $q = 0.00860$. The flow fields

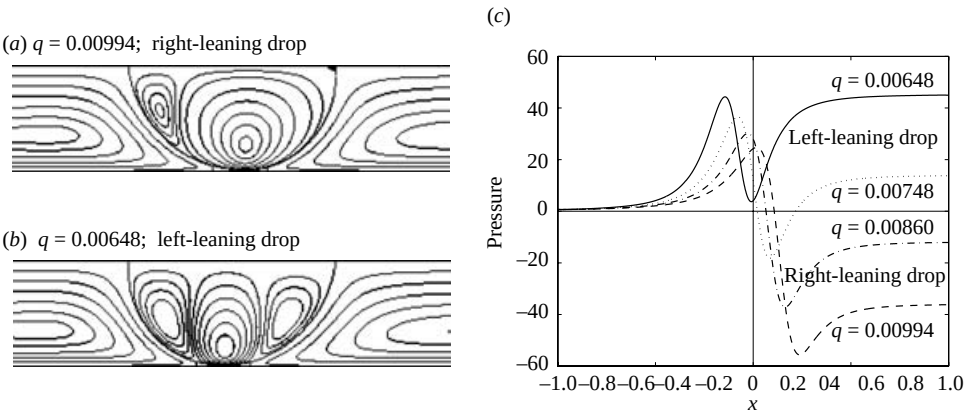

FIGURE 4. (*a*, *b*) Streamlines of the flow field from the FEMLUB model using a silicone-oil drop and air with $d = 1.01$, $Re = 23.756$, and two different flow rates. (*c*) The pressure versus x along the drop interface for four different flow rates.

are very similar (note that the streamline contour values are not the same). Kuo *et al.*'s maximum tangential speed on the drop interface is $V_s = 0.0387$ occurring at $x = 0.06$, while the FEMLUB model has $V_s = 0.0419$ occurring at $x = 0.069$, an 8.3% velocity difference. Kuo *et al.* reported that the two zero-velocity points on the interface occurred at $x = -0.35$ and 0.60, while the FEMLUB model shows $x = -0.40$ and 0.75. Finally, the minimum film thickness estimated from Kuo *et al.*'s results is $h_{min} = 0.012$ at $x = 0.05$, while it is $h_{min} = 0.0122$ at $x = 0.073$ in the present results. Overall, the results from the two models agree quite well.

Figure 3(*c*) shows the pressure along the lower surface of the channel. This curve displays the characteristic maximum and minimum structure found in similar lubrication problems, such as forward-roll coating (see Smith 1997). The pressure increases rapidly as the moving lower surface drags gas into the space beneath the drop. Just to the left of the point of minimum film thickness the pressure peaks and then drops rapidly. As the film thickness increases, the pressure reaches a minimum and then rises again. Away from the influence of the drop, the pressure gradients at each end of the channel are constant and equal. If these gradients are extrapolated to intersect the y-axis at the centre of the channel (see figure 3*c*), the distance between the top and bottom intersection points defines an effective pressure drop Δp_{eff} for the flow past the drop as follows:

$$\Delta p_{eff} = p_L - p_R + w p_x, \tag{3.1}$$

where p_L and p_R are the pressures at each end of the channel, w is the channel width, and p_x is the constant pressure gradient at each end of the channel. Likewise, the horizontal distance between the constant-pressure-gradient lines as they intersect any horizontal line defines an effective channel width w_{eff}, which is given by the relation

$$w_{eff} = \Delta p_{eff}/p_x = w + (p_L - p_R)/p_x. \tag{3.2}$$

The effective width is useful because it defines a finite two-dimensional channel/drop system centred at the origin with a Couette–Poiseuille flow and the same pressure at each end. The effective pressure drop and width for the flow in figure 3(*a*) are $\Delta p_{eff} = 13.50$ and $w_{eff} = 55.42$.

Figures 4(*a*) and 4(*b*) show the streamlines for flows with $d = 1.01$, $Re = 23.756$, and $q = 0.00994$ and $q = 0.00648$, respectively. These figures show that the drop is pushed

to the right for larger values of the flow rate and to the left for smaller values. The reason for this behaviour lies in the net force on the drop. The dominant source of the horizontal shear force on the drop is the moving lower surface. As it drags gas to the right and under the drop by viscous stresses, it creates a positive (rightward) shear force on the drop. For a system with no top solid surface, in which the drop is lowered toward the moving solid surface, this viscous shear force in the lubrication domain is the dominant force on the drop. Such is the case in the experiments of Neitzel & Dell'Aversana (2002). However, in this channel system with a fixed upper solid surface, the pressure force on the drop interface is the dominant horizontal force. The horizontal viscous shear force is on the order of 4% of the pressure force when $d = 1.01$. Figure 4(c) shows gas pressure distributions along the drop interface for four different values of the flow rate, two of which are for the cases depicted in figures 4(a) and 4(b). For ease of comparison, the location of the zero-point reference pressure for all of these pressure distributions is shifted to the left end of the channel, i.e. $p(x = -4) = 0$. For both left- and right-leaning drops, the pressure rises sharply as the gas approaches the drop from the left side, there is a pressure maximum followed by a large pressure drop to a minimum in the lubrication zone, and finally the pressure rises as the gas moves away from the drop on the right-hand side. For larger values of the flow rate (figure 4(c), $q = 0.00994$), the pressure on the right side of the drop is lower than that on the left. Thus, the drop leans to the right since both pressure and viscous shear forces act in the same direction. For smaller values of the flow rate (figure 4(c), $q = 0.00648$), the pressure rise on the right-hand side of the drop is larger and the pressure on the right exceeds the pressure on the left. When this negative pressure force exceeds that of the viscous shear force, the drop leans to the left, in the direction opposing the motion of the lower surface.

For another explanation of this effect, consider the positive pressure gradient that exists within the gas far enough away from the drop and on both sides of the channel. This pressure gradient drives the required flow to the left along the upper wall and regulates the flow rate. If the pressure at the left end of the channel is set to zero, then to decrease the flow rate the pressure at the right end must increase. This pressure increase translates directly to the pressure rise on the right side of the drop seen in figure 4(c) for decreasing flow rates.

The net horizontal and vertical forces on the drop are plotted in figure 5 as a function of the flow rate for a fixed Reynolds number, and as a function of the Reynolds number for a fixed flow rate. For $q \geqslant 0.00860$, the drop leans to the right, while for $q \leqslant 0.00748$, the drop leans to the left. Also note that the vertical force on a right-leaning drop is downward. This force is dominated by the large suction pressure on the right side of the lubrication domain. The vertical force on a left-leaning drop is upward (except when the flow rate is near the value $q = 0.00748$), and it is dominated by the large positive pressure on the left side of the lubrication domain.

The most interesting feature of figure 5(a) is that no solutions were found in the interval $0.00748 < q < 0.00860$. Recall that with the flow rate fixed, the drop-shape iteration history showed time-like oscillations in the drop shape. This prompted the use of the relation $q = kh_{min}$ to compute the flow rate and fixing the value of the parameter k during the iteration. If the horizontal drop force in figure 5(a) is re-plotted versus the parameter k, the left and right portions of the curve become the lower and upper parts of a typical S-shaped hysteresis curve. The upper turning point corresponds to the flow rate $q = 0.00860$ and the lower turning point corresponds to the flow rate $q = 0.00748$. It seems that the flow-rate interval between these two values corresponds to the unstable branch connecting the two turning points. Thus,

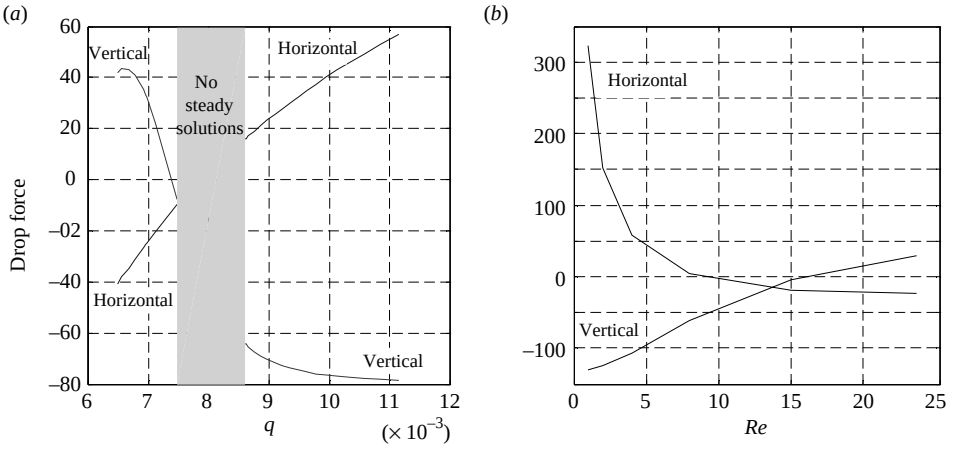

FIGURE 5. The horizontal and vertical force on the drop from the FEMLUB model using a silicone-oil drop and air with $d = 1.01$. (*a*) $Re = 23.756$, and (*b*) $q = 0.00700$. The grey band denotes the interval $0.00748 < q < 0.00860$ where no steady solutions are found.

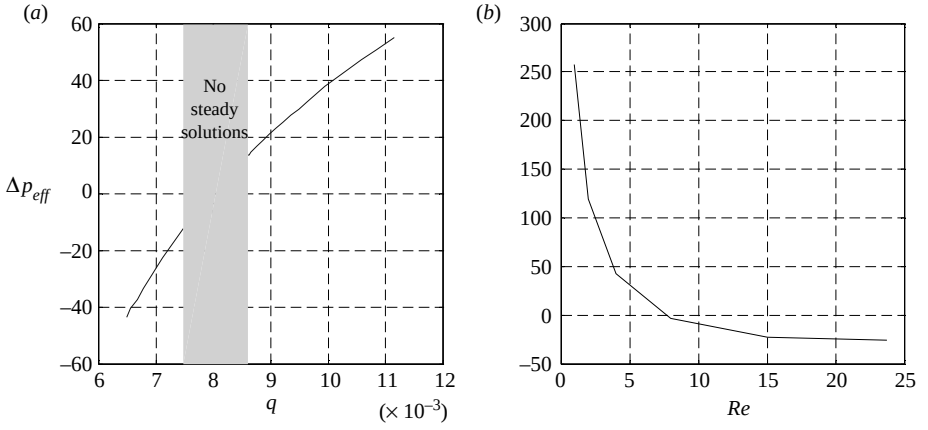

FIGURE 6. The effective pressure drop for the flow past the drop from the FEMLUB model using a silicone-oil drop and air with $d = 1.01$. (*a*) $Re = 23.756$, and (*b*) $q = 0.00700$. The grey band denotes the interval $0.00748 < q < 0.00860$ where no steady solutions are found.

for these flow rates one might expect to find unstable transient solutions in which the drop exhibits a side-to-side oscillation.

Figure 5(*b*) shows the dependence of the drop forces on the Reynolds number for a fixed flow rate $q = 0.00700$. For small values of the Reynolds number, the drop leans to the right and the vertical force is downward. The horizontal force is negative and the drop leans to the left for Reynolds numbers $Re > 8$. The vertical force becomes positive for Reynolds number $Re > 16$. Note that increasing the Reynolds number is equivalent to increasing the speed of the lower surface. Thus, increasing the lower-surface speed to the right leads to a shift in the position of the drop to the left.

Figure 6(*a*) shows the effective pressure drop Δp_{eff} in the channel as a function of the flow rate. As expected, this pressure drop increases with increasing flow rate. It is usually positive (negative) when the drop leans to the right (left). Figure 6(*b*) shows

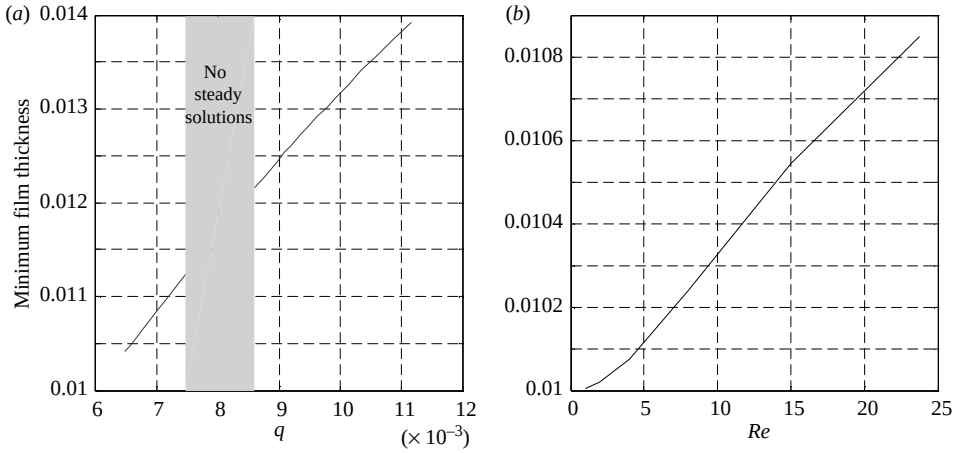

FIGURE 7. The minimum film thickness under the drop from the FEMLUB model using a silicone-oil drop and air with $d = 1.01$. (*a*) $Re = 23.756$, and (*b*) $q = 0.00700$. The grey band denotes the interval $0.00748 < q < 0.00860$ where no steady solutions are found.

FIGURE 8. The streamlines for the flow field from the FEMLUB model using a silicone-oil drop and air with $d = 0.93$, $Re = 23.756$, and $q = 0.00256$. This is not a converged steady solution.

that increasing the Reynolds number for a fixed flow rate decreases the effective pressure drop. An increased Reynolds number implies an increase in the speed of the lower surface, which acts to assist the transport of gas underneath the drop. The effective pressure drop is a measure of the pressure force across the drop required to force the gas under and past the drop. It is much easier to flow beneath the drop when the lower surface is moving faster and assisting in the transport. Thus, the effective pressure drop decreases with increasing Reynolds number.

The minimum film thickness under the drop is shown in figure 7. It increases with increasing flow rate and Reynolds number, although the increase is much larger with the flow rate for this range of parameters.

The FEMLUB model also works well when the surface-separation distance $d < 1$. Unfortunately, for this two-dimensional channel system no steady solutions were found when $d < 1$ for either left- or right-leaning drops. The iteration history for every parameter set examined exhibits under-relaxed monotonic or oscillatory changes in the drop shape, most of which eventually lead to the drop interface intersecting the lower surface. This kind of behaviour indicates that a steady drop shape is probably unstable when $d < 1$ and that the drop will eventually wet the lower solid surface. These unsteady solutions are beyond the scope of the present model.

Figure 8 shows the streamlines for the flow past the drop for $d = 0.93$ and $Re = 23.756$ at one point in its oscillatory iteration history. This is not a converged solution. The figure is only intended to show that the FEMLUB model does compute the flow field and the drop shape for these severely squeezed drops. The horizontal and vertical forces on the drop and the effective pressure are $F_x = -121.9$, $F_y = 190.9$, and $\Delta p_{eff} = -139.4$. All of these values are about an order of magnitude larger than

those for a drop with $d = 1.01$ and the same Reynolds number (see figures 5 and 6). This result gives some indication of how the forces in the flow increase as the drop is squeezed toward the lower surface. The minimum film thickness for this iteration is $h_{min} = 0.00479$. For a 1 mm drop, this gives a minimum film thickness of about 5 μm, which is a typical value seen in the experiments of Dell'Aversana & Neitzel (2004).

4. Conclusions

Isothermal non-wetting of a liquid drop attached to a fixed solid surface and pressed against a second parallel solid surface moving in its own plane has been demonstrated numerically in a two-dimensional setting. FEMLUB, a hybrid finite-element/lubrication-theory model constructed with the FEMLAB finite-element software, solved the complete deformable interface problem for the gas flow in the channel, the flow in the liquid drop, and the shape of the drop. The effects of the surface separation distance, the Reynolds number, and the flow rate of the gas in the channel were examined in some detail.

The system displays several interesting behaviours. When the drop is close enough to the lower moving surface ($d \leqslant 1.01$) there is a range of flow rates for which no steady solutions are possible. For smaller (larger) flow rates, the drop leans to the left (right). The effective pressure drop is a measure of the pressure force on the drop required to drive the gas flow in the lubrication film underneath the drop. It increases with increasing flow rate and decreases with increasing Reynolds number. For a small enough Reynolds number, the drop leans to the right. Increasing the Reynolds number causes the drop to lean to the left, opposite to the direction of the moving lower surface. As a rule of thumb, right (left)-leaning drops experience a downward (upward) vertical force. The minimum film thickness underneath the drop increases with increasing flow rate and Reynolds number.

When the two solid surfaces are closer together than the radius of the undisturbed drop, no steady drop-shape solutions were found. However, a typical unconverged drop shape solution for the flow field shows that the magnitudes of the forces and effective pressure drop are about an order of magnitude larger than when $d = 1.01$. Lastly, the minimum film thickness decreases from 0.01042 for $d = 1.01$ to 0.00479 for $d = 0.93$.

The future direction for this work is to extend the hybrid technique to three dimensions. The primary three-dimensional effect is to allow the gas to flow around the drop. This would minimize the large suction pressure beneath the drop and probably result in an upward vertical force on the drop for all conditions, as seen in experiments. It is also possible that this extension would allow steady drop shapes to be found when the surface separation distance is less than the radius of the undisturbed drop.

G. P. Neitzel gratefully acknowledges support of this work by the NASA Office of Biological and Physical Research.

REFERENCES

Chen, J.-C., Kuo, C.-W. & Neitzel, G. P. 2006 Numerical simulation of thermocapillary nonwetting. *Intl J. Heat Mass Transfer* (to appear).

Dell'Aversana, P. & Neitzel, G. P. 2004 Behavior of noncoalescing and nonwetting drops in stable and marginally stable states. *Exps. Fluids* **36**, 299.

Dell'Aversana, P., Tontodonato, V. & Carotenuto, L. 1997 Suppression of coalescence and wetting: the shape of the interstitial film. *Phys. Fluids* **9**, 2475.

Hadjiconstantinou, N. G. 1999 Hybrid atomistic-continuum formulations and the moving contact-line problem. *J. Comput. Phys.* **154**, 245.

Kuo, C.-W., Chen, J.-C. & Neitzel, G. P. 2005 Numerical simulation of isothermal nonwetting. *Intl J. Numer. Meth. Fluids* (submitted).

Monti, R. & Savino, R. 1997 Correlation between experimental results and numerical solutions of the Navier-Stokes problem for noncoalescing liquid drops with Marangoni effects. *Phys. Fluids* **9**, 260.

Nalevanko, J. C. 1997 Design of an apparatus for investigation of 2-D liquid drop non-coalescence. M.S. Thesis, The George W. Woodruff School of Mechanical Engineering, Georgia Institute of Technology.

Neitzel, G. P. & Dell'Aversana, P. 2002 Noncoalescence and nonwetting behavior of liquids. *Annu. Rev. Fluid Mech.* **34**, 267.

Rayleigh, Lord 1879 On the capillary phenomena of jets. *Proc. R. Soc. Lond.* A **29**, 71.

Ruschak, K. J. 1982 Boundary conditions at a liquid-air interface in lubrication flows. *J. Fluid Mech.* **119**, 107.

Savino, R. & Monti, R. 1997 Modelling of non-coalescing liquid drops in the presence of thermocapillary convection. *Meccanica* **32**, 115.

Smith, M. K. 1997 Asymptotic methods for the mathematical analysis of coating flows. In *Liquid Film Coating, Scientific Principles and their Technological Implications* (ed. S. F. Kistler & P. M. Schweizer), pp. 251–296. Chapman & Hall.

Stay, M. S. & Barocas, V. H. 2003 Coupled lubrication and Stokes flow finite elements. *Intl J. Numer. Meth. Fluids* **43**, 129.

Sumner, L. B. S., Wood, A. M. & Neitzel, G. P. 2003 Lubrication analysis of thermocapillary-induced nonwetting. *Phys. Fluids* **15**, 2923.